Journal of Catalysis **197,** 17–25 (2001)
doi:10.1006/jcat.2000.3061, available online at http://www.idealibrary.com on IDEAL®

Kinetics of Butane Oxidation by a Vanadyl Pyrophosphate Catalyst

Daxiang Wang and Mark A. Barteau[1]

Center for Catalytic Science and Technology, Department of Chemical Engineering, University of Delaware, Newark, Delaware 19716

Received February 21, 2000; revised August 11, 2000; accepted August 15, 2000

The kinetics of butane oxidation by a vanadyl pyrophosphate (VPO) catalyst were analyzed from reduction transients using a novel oscillating microbalance reactor. The reduction rate of the equilibrated VPO catalyst with butane is 0.4th order in the butane concentration and 4th order in the available lattice oxygen concentration. This rate law is effective in representing the reduction of the catalyst to an extent equivalent to the removal of several layers of lattice oxygen. The activation energy for the reduction process is 85 kJ/mol, nearly the same as the apparent activation energy for the steady-state oxidation of butane on the VPO catalyst. These results suggest that the activation of butane is the rate-determining step for butane oxidation on VPO catalysts and that four surface oxygen ions may be involved in this step. The kinetics of VPO reduction by butane are useful in predicting the oxygen capacity of the catalyst and rate of butane oxidation under cyclic feed conditions, as in the circulating fluidized bed process.

Key Words: **VPO catalyst; kinetics; transient reaction; oxidation of butane; maleic anhydride.**

INTRODUCTION

A new industrial process for the production of maleic anhydride (MA) by selective oxidation of butane on vanadyl pyrophosphate (VPO) catalysts with a circulating fluidized bed reactor was commercialized recently (1). In this process, the vanadyl pyrophosphate catalyst works as an oxygen carrier, transferring oxygen from a regenerator to a riser reactor where butane is selectively oxidized to maleic anhydride; the reduced catalyst is then circulated back to the regenerator to be regenerated by oxidation with air (2–4). The oxygen availability and the effectiveness of the reversible restoration of the catalyst lattice oxygen in the redox cycle are critical factors determining the economic feasibility of such technology (5–8). In a previous paper we reported results identifying the vanadium species involved in the sequential redox operation of the VPO catalyst (9). In this study, the kinetics of butane oxidation on an oxidized VPO catalyst are investigated.

The kinetics for butane oxidation to MA on VPO catalysts have been thoroughly investigated under steady-state reaction conditions in which butane and oxygen are co-fed (10–21). The main observation is that the oxidation reaction follows a redox mechanism, with the rate of butane consumption adequately represented by power rate law. There appears to the general agreement that the reaction rate for co-fed oxygen and butane is first order in butane. Controversies exist regarding the activation energy and the reaction order with respect to oxygen. Values reported for the activation energy range from 40 to 150 kJ/mol; the reaction order in gas phase oxygen varies between 0 and 1 (10–21). Centi *et al.* (17) attributed the surprising uncertainty in the reported values of the activation energy and the reaction order in oxygen to the sensitivity of the oxidation reaction to the catalyst structure. On a newly activated, active, nonequilibrated VPO catalyst it is suggested that, because of the existence of crystal defects, the catalyst is more susceptible to oxidation and the lattice oxygen is more active. Hence, such a catalyst usually exhibits a lower reaction order (0–0.5) in oxygen and a smaller activation energy (11–13, 18, 19). In contrast, on a stable catalyst, the activation energy is higher and the reaction order in oxygen is close to 1 (20, 21). Because of this apparent structure sensitivity of the kinetics, it is problematical to use literature data to predict non-steady-state or cyclic reactor operation. Therefore, in this study, measurements of the activation energy were made by both steady-state and transient methods to permit their direct comparison.

In studying the transient reaction kinetics of butane on VPO catalysts, we can simplify the data analysis by avoiding the interference of gas phase oxygen. The kinetics thus obtained may provide more information about the reaction mechanism and may be more representative of the reducing operating regions of the circulating fluidized bed reactor scheme.

EXPERIMENTAL METHODS

Catalyst Preparation

The performance of VPO catalysts depends strongly on their preparation. In this study, the catalyst precursor, vanadyl hydrogen phosphate hemihydrate ($VOHPO_4 \cdot 0.5\ H_2O$), was synthesized by refluxing V_2O_5 (Aldrich) in a

[1] To whom correspondence should be addressed. Fax: 302-831-8201. E-mail: barteau@che.udel.edu.

0021-9517/01 $35.00

mixture of isobutanol (Aldrich) and H_3PO_4 85% (Fisher) ($P/V = 1.0$) at 100°C for 16 h (9, 22). The precipitate was washed thoroughly with isobutanol and ethanol until the filtrate became clear and colorless. This precursor was dried at room temperature for 2 h and then at 110°C overnight.

Catalyst Characterization

The phase structure of the catalyst precursor and the activated catalyst was examined with X-ray diffraction (XRD) on a X'PERT diffractometer using Cu$K\alpha$ radiation at 40 kV and 55 mA. The XRD measurements were carried out at ambient conditions. BET surface areas were analyzed by nitrogen adsorption at 77 K.

Steady-State Reaction Experiments

The catalyst performance was tested in a continuous flow, fixed bed tubular reactor operating at atmosphere pressure. The reactor is a 25-cm-long, 6-mm-od quartz tube which was flared to 13 mm in the center over a distance of 2 cm. The catalyst sample was packed in the flared portion and quartz chips were loaded on both sides to minimize gas phase reactions. *In situ* catalyst activation was carried out with the tubular reactor by heating 1.7 g of the precursor in a gas mixture of butane/oxygen/He (1.75%/21%/balance) from 30 to 400°C at 2°C/min and then holding at 400°C for 24 h. The reactant was prepared by blending 10 vol% butane/He (Matheson Gas) with oxygen (Matheson purity) and helium (Keen Gas, Grade 5). The total flow rate was 50 ml/min. Butane conversion and product selectivities were measured with an on-line GC (HP5890 II Plus). Butane and MA were detected with a flame ionization detector after separation with a capillary column, HP-5, 0.32 mm × 30 m. Oxygen, butane, and carbon oxides were detected with thermal conductivity detectors after separation with two parallel columns, viz., an 8-ft Haysep Q column (for hydrocarbons and carbon dioxide) and a 10-ft molecular sieve 13X column (for oxygen and carbon monoxide).

Kinetics Study

The kinetics of the steady-state reaction of butane/oxygen/He on the VPO catalyst, as well as the transient reaction of butane on the pretreated VPO catalyst, were investigated with a novel oscillating microbalance reactor. The instrument setup and its features have been described previously (9, 23–25).

To determine the activation energy for the steady-state reaction of butane/oxygen on the VPO catalyst, the microbalance reactor was operated as a differential fixed bed reactor loaded with 100 mg of preactivated VPO catalyst. A gas mixture containing butane/oxygen/Ar/He (1.75/21/1.64/balance) flowed through the reactor at 50 ml/min at atmospheric pressure. Butane conversion was monitored with an on-line quadrupole mass spectrometer (UTI 100C). The most abundant fragment of butane at $m/e = 43$ was used to measure the butane concentration and $m/e = 40$ for argon was used as an internal standard.

In the measurement of the transient reaction kinetics, the reactor loaded with 100 mg of activated VPO catalyst was heated up to 400°C at 10°C/min in a gas mixture of butane/oxygen/He = 1.75/21/balance at 50 ml/min under atmospheric pressure. After 2 h of reaction under the above conditions, the catalyst was purged with helium (Keen Gas, Grade 5, further purified with an oxygen trap) for 30 min at 400°C or cooled to the desired temperature under the purge of helium. The reaction of butane on this reaction-equilibrated catalyst was then started by turning on the gas mixture of butane/He (0.4–2.4 vol% butane in helium). Reductions were carried out at several different temperatures between 340 and 400°C.

RESULTS

Phase Structures

The XRD pattern of the catalyst precursor (Fig. 1) shows a pure, well-crystallized $VOHPO_4 \cdot 0.5\ H_2O$ (26, 27). Figure 2 is the XRD pattern of the catalyst after 24-h activation at 400°C; all of the strong peaks can be assigned to vanadyl pyrophosphate (26, 27). The strongest peak at $2\theta = 23.0$ corresponds to reflections from [200] crystal planes. It suggests that vanadyl pyrophosphate crystal planes are stacked preferentially along the [100] direction. The BET surface area of the activated catalyst is 16.9 $m^2\,g^{-1}$.

Reaction of Butane with Co-fed Oxygen on the Equilibrated VPO Catalyst

When the catalyst precursor was activated *in situ*, its performance became stable after several hours on stream. The reaction data obtained at steady state are listed in Table 1.

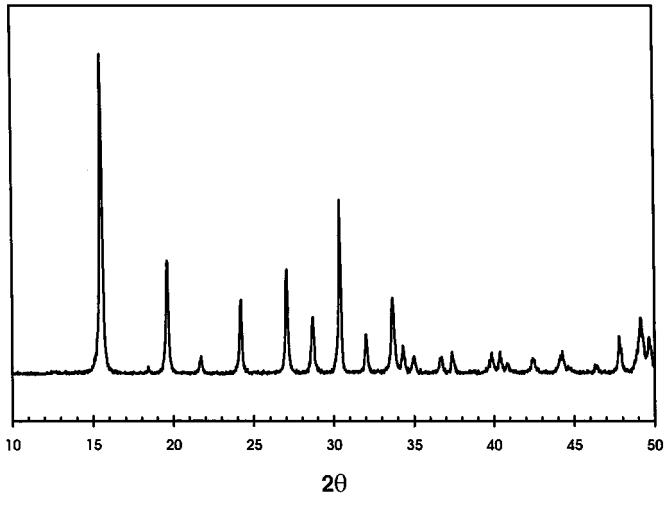

FIG. 1. XRD pattern of the catalyst precursor, $(VO)HPO_4 \cdot 0.5\ H_2O$.

TABLE 1

Butane Oxidation on Vanadyl Pyrophosphate in an Integral Fixed Bed Reactor[a]

Temperature (K)	Conversions (%)		Selectivities (%)		
	Butane	Oxygen	MA	CO	CO_2
616	19	5	66	8	25
638	30	9	63	10	27
653	44	13	61	11	28
674	59	19	58	12	29
699	77	26	54	15	31

[a] Total flow rate: 50 ml/min; Mass of catalysts: 1.7 g precursor; Gas composition: butane/oxygen/He = 1.75/21/balance.

In general the butane conversions and product selectivities listed in Table 1 are very typical for butane oxidation on well-crystallized VPO catalysts. Under the current experimental conditions, the highest selectivity to MA was about 66% at 19% butane conversion that was obtained at 616 K. At comparable butane conversions, the selectivity to MA obtained in this study is slightly lower than that obtained previously on a VPO catalyst with P/V ratios of 1.08 (9). This result follows the common trend that lower P/V ratios improve catalyst activity at the expense of decreasing selectivity to MA (28).

Table 1 also shows that, with the increase of reaction temperature, butane conversion increased, but the selectivity to MA decreased somewhat. The decrease of MA selectivity at high temperatures can be attributed to the degradation of MA at high butane conversion (29–35).

Table 2 illustrates the catalytic performance of the equilibrated VPO catalyst for the reaction of butane/oxygen/Ar/He obtained with the microbalance reactor at a gas space velocity of 30,000 ml h^{-1}(g cat)$^{-1}$. Due to the high space velocity, butane conversions were relatively low at all temperatures, ranging from 2.6 to 12% at 343–400°C. Thus the flow microbalance can be considered to operate as a differential reactor, and the concentrations of the reactants along the catalyst bed can be assumed to be constant.

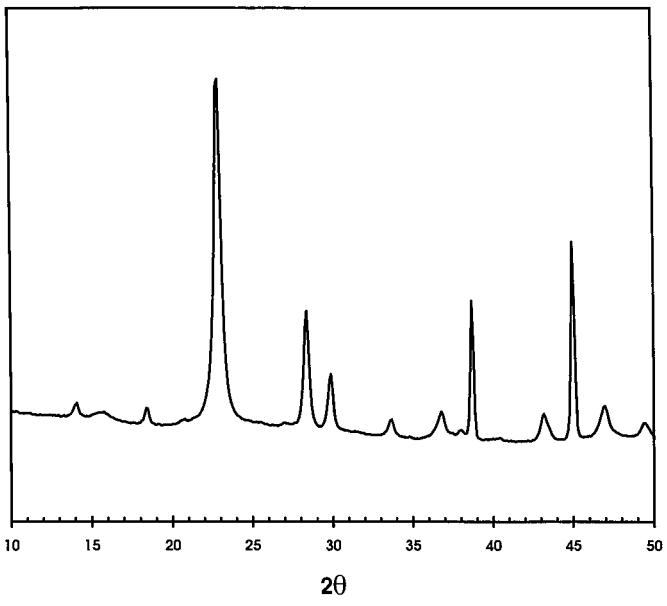

FIG. 2. XRD pattern of the activated catalyst, $(VO)_2P_2O_7$.

Moreover, operation at differential conversion also simplifies the kinetics analysis by eliminating the need to consider the possible sequential oxidation of maleic anhydride (18). As shown in Table 1, the selectivity to maleic anhydride decreases by less than 20% as the butane conversion is increased from 19 to 77%. This indicates that the rate constant for sequential oxidation of maleic anhydride is much less than that for butane oxidation. Thus maleic anhydride oxidation can be neglected at the low butane conversions examined in the microbalance experiments.

The reaction rates at each temperature were calculated from the butane conversions, the initial concentration of the reactants (butane/oxygen/Ar/He = 1.75%/21%/1.64%/balance), and the total gas flow rate (50 ml min^{-1}). The results are listed in Table 2 in mol h^{-1} g^{-1}, mol h^{-1} m^{-2}, and turnover frequency (s^{-1}). The turnover frequency was calculated based on the surface vanadium density of 8.4 μmol/m^2 on the [100] crystal plane of vanadyl

TABLE 2

Butane Oxidation on Vanadyl Pyrophosphate in a Differential Fixed Bed Reactor[a]

Temperature (K)	Butane conversion (%)	Oxidation reaction rate		
		10^{-4} mol h^{-1} g^{-1}	10^{-5} mol h^{-1} m^{-2}	TOF (10^{-3} s^{-1})
616	2.6	6.1	3.6	1.2
636	4.3	10	5.9	2.0
655	5.8	13.6	8.0	2.6
673	12	28	16.6	5.5

[a] Gas composition: butane/oxygen/Ar/He = 1.75%/21%/1.62%/balance; Total flow rate: 50 ml/min. Mass of activated catalyst: 100 mg with BET surface area of 16.9 m^2/g.

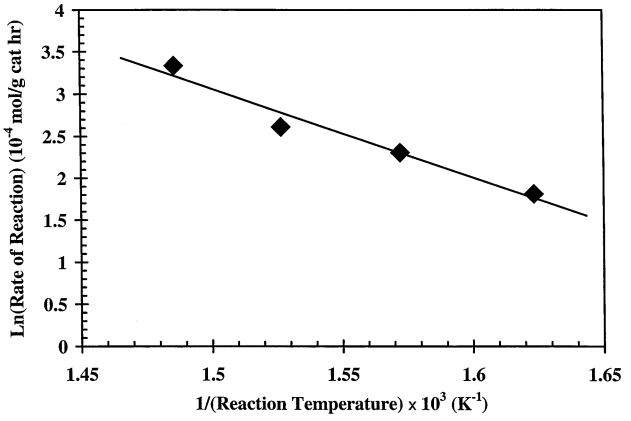

FIG. 3. Arrhenius plot of steady-state butane oxidation on the VPO catalyst.

pyrophosphate (26) and the BET surface area of 16.9 $m^2 g^{-1}$ for the sample tested. At the very low turnover frequencies characteristic of the current experimental conditions, one would expect the reaction to be controlled by the intrinsic kinetics.

Figure 3 presents the Arrhenius plot of $\ln(r)$ versus $1/T$, where r is the oxidation rate of butane in units of 10^{-4} mol h^{-1} (g cat)$^{-1}$. The apparent activation energy thus calculated was 88 kJ/mol for butane oxidation with co-fed oxygen on the VPO catalyst.

Transient Reaction of Butane/He on the Equilibrated VPO Catalyst

When a vanadyl pyrophosphate catalyst is operated under steady-state oxidation conditions in a gas mixture of butane and oxygen with a molar ratio of oxygen to butane of about 12, the catalyst is in an oxidized state (9). When the feed over such a catalyst is switched to butane, butane will be oxidized and the catalyst will be reduced. Figure 4 shows the experimental results from the microbalance reactor for the reaction of butane on the equilibrated VPO catalyst. It records the mass changes of the VPO catalyst with time on stream upon reduction in butane/He. Several gas compositions were used to determine the reaction order in butane. The mass change is shown relative to the stable mass of the catalyst under helium purge at the same temperature, after reaction equilibration at 400°C for 2 h in a gas mixture of butane/oxygen/He (1.75/21/balance).

When the gas was switched from pure helium to butane/He, there was a rapid change in the apparent mass of the catalyst bed due to the buoyancy effect caused by the density difference between the gases. This apparent mass change occurs on a time scale of the order of seconds (the total flow rate of the reduction gas is 50 ml/min, which results in a residence time of 1.2 s in the catalyst bed of 0.1 ml). The data plotted in Fig. 4 have been corrected for this buoyancy effect. As was demonstrated previously (9), there is little physisorption of reactants and/or products or carbon deposition on the catalyst under these conditions. For example, switching butane in or out of the helium flow to a catalyst at 235°C (below the temperature at which butane oxidation occurs) produced apparent mass changes that were completely reversible and that were entirely consistent with the effect of the change in gas density. Likewise, experiments in which the effluent from the reactor was monitored with the mass spectrometer during oxidation of a catalyst previously reduced in butane showed relatively little evolution of carbon oxides. Quantification of these levels demonstrated that the deposition of carbonaceous species could account for less than 5% of the catalyst mass change during the reduction process, even for several hours of reduction in butane. Thus the mass changes recorded in Fig. 4 are solely an indication of the removal of oxygen from the catalyst.

The overall network of oxidation reactions for butane and products on a VPO catalyst can be described by

$$C_4H_{10} + \alpha[O]\,(\text{lattice}) \rightarrow \beta MA\,(\text{gas}) + \chi CO_x\,(\text{gas}) + \delta H_2O\,(\text{gas}) + \alpha[*] \quad [1]$$

$$MA + \varepsilon[O]\,(\text{lattice}) \rightarrow \phi CO_x\,(\text{gas}) + \varepsilon[*] \quad [2]$$

$$CO + \gamma[O]\,(\text{lattice}) \rightarrow CO_2\,(\text{gas}) + \gamma[*], \quad [3]$$

where α, β, χ, δ, ε, ϕ, and γ are the stoichiometric numbers for the corresponding reactants and/or products. [O] and [$*$] represent lattice oxygen and lattice oxygen vacancies, respectively.

All of the above three reactions result in the consumption of lattice oxygen and hence contribute to the catalyst mass change. The mass change rate of the catalyst according to

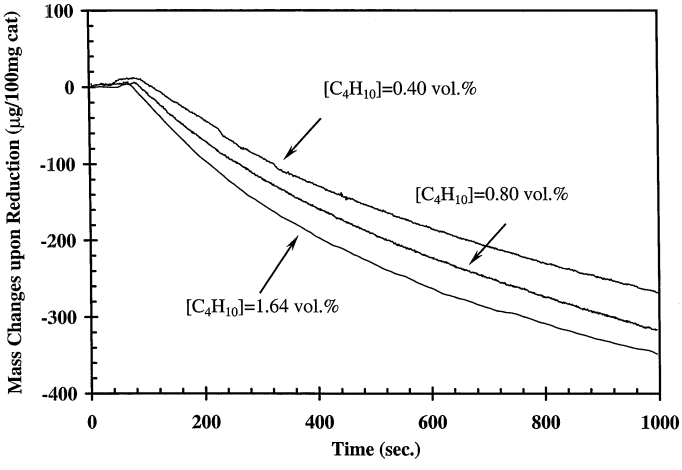

FIG. 4. Isothermal reduction of the equilibrated VPO catalyst in butane/He. Conditions: 100 mg VPO catalyst, temperature = 400°C, SV = 30,000 ml h^{-1}(g cat)$^{-1}$; butane concentrations are as indicated.

reactions [1]–[3] can be described as

$$-dm/dt = \Psi \cdot (-d[\mathrm{O}]/dt) = k_1 \cdot [\mathrm{C_4H_{10}}]^a \cdot [\mathrm{O}]^b + k_2 \cdot [\mathrm{MA}]^c \cdot [\mathrm{O}]^d + k_3 \cdot [\mathrm{CO}]^e \cdot [\mathrm{O}]^f. \quad [4]$$

$[C_4H_{10}]$, [O], [MA], and [CO] are the concentrations of butane (vol%), lattice oxygen (mol [O] m^{-2}), MA (vol%), and carbon monoxide (vol%), respectively. k_1, k_2, and k_3 are the reaction rate constants for reactions [1] through [3], respectively. ψ is a calibration constant compensating for the difference in units between $-dm/dt$ and $d[\mathrm{O}]/dt$. The mass change rate in g (g cat)$^{-1}$ s^{-1} is expressed as $-dm/dt$; "$-d[\mathrm{O}]/dt$" is the reaction rate expressed as the consumption of lattice oxygen in mol m^{-2} s^{-1}. The exponents *a*, *b*, *c*, *d*, *e*, and *f* are the reaction orders with respect to the corresponding reactants.

Under the current transient experimental conditions, butane oxidation was carried out in a differential mode. For example, butane conversion is 12% at 400°C in a gas mixture of butane/oxygen/Ar/He (1.75/21/1.62/balance), as listed in Table 2. The butane conversion for a gas without co-fed oxygen should be lower, i.e., under transient reaction conditions, butane conversions are always much less than 12%. Therefore, the concentrations of maleic anhydride and carbon monoxide are relatively low throughout the reactor compared with the butane concentration. As demonstrated above and elsewhere (10–13), MA is much less reactive than butane on the VPO catalyst. Separate experiments also showed that the reduction of the oxidized VPO catalyst by CO was approximately two orders of magnitude slower than reduction by butane. Thus, under the differential butane conversions obtained in our microbalance experiments, the last two terms in rate equation [4] can be omitted and Eq. [4] can be simplified as

$$-dm/dt = \Psi \cdot (-d[\mathrm{O}]/dt) = k_1 \cdot [\mathrm{C_4H_{10}}]^a \cdot [\mathrm{O}]^b. \quad [5]$$

The kinetic parameters in rate expression [5] can be calculated based on the experimental results.

The initial reduction rates were measured as the slope of the mass change at the beginning of each reduction from the experimental data shown in Fig. 4. The initial reduction rates obtained are listed in Table 3. The reductions shown in Fig. 4 were all carried out at similar temperatures and followed similar pretreatment procedures. The initial reduction rate depends only on the butane concentration in the feed. There is a linear dependence of $\ln(-dm/dt)$ on $\ln([C_4H_{10}])$, as shown in Fig. 5. The reaction order in butane thus obtained is 0.4.

The rate constant k_1 in Eq. [5] should have an Arrhenius dependence on reaction temperature. This dependence was also measured with the microbalance reactor. Figure 6 depicts the experimental results for the reduction of equilibrated VPO catalyst in 0.8 vol% butane in helium at several

TABLE 3

Effect of Butane Concentration on the Reduction Rate of the VPO Catalyst[a]

Butane concentration (vol%)	Rate of reduction ($\times 10^{-7}$ g[O] s^{-1} (g cat)$^{-1}$)
0.4	4.9
0.8	6.7
1.64	8.6
2.4	10.2

[a] The reduction rate was measured from the slope of mass change at the beginning of the reduction. Reaction temperature: 673 K; the reactant is butane balanced with helium, 50 ml/min.

different temperatures. The initial reduction rates at each temperature are listed in Table 4. Because of the similar pretreatment procedures for the VPO catalyst prior to each reduction, the starting states of the VPO catalyst for each reduction are all the same, i.e., the lattice oxygen concentrations, [O], are similar at the beginning of each reduction. By plotting $\ln(-dm/dt)$ versus $1/T$ (Fig. 7), the apparent activation energy for the reduction reaction was estimated as 85 kJ/mol.

Let us now calculate the reaction order, *b*. This parameter can be estimated by integration of rate equation [5] and regression of data from Fig. 4 with the integrated equation. Under certain temperatures and butane concentrations, Eq. [5] can be rewritten

$$-dm/dt = \Psi \cdot (-d[\mathrm{O}]/dt) = f\ (T, [\mathrm{C_4H_{10}}]) \cdot [\mathrm{O}]^b, \quad [6]$$

where $f\ (T, [C_4H_{10}])$ is a function of temperature and

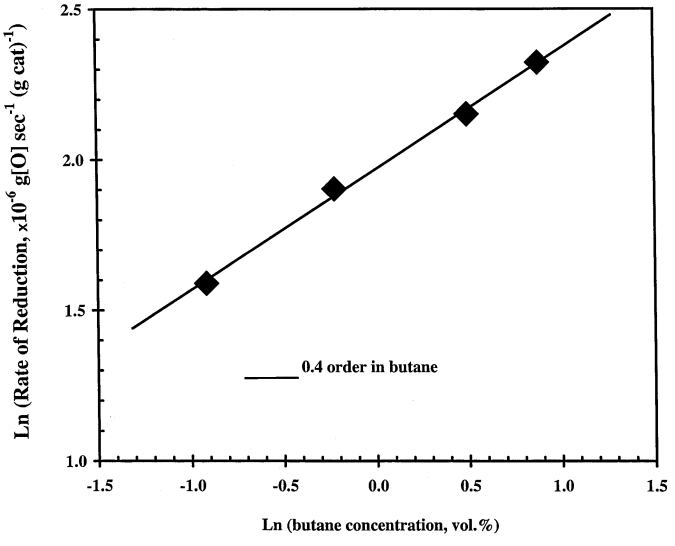

FIG. 5. Determination of reaction order on butane for the reduction of the equilibrated VPO catalyst. Conditions: 100 mg VPO catalyst, temperature = 400°C, SV = 30,000 ml h^{-1}(g cat)$^{-1}$.

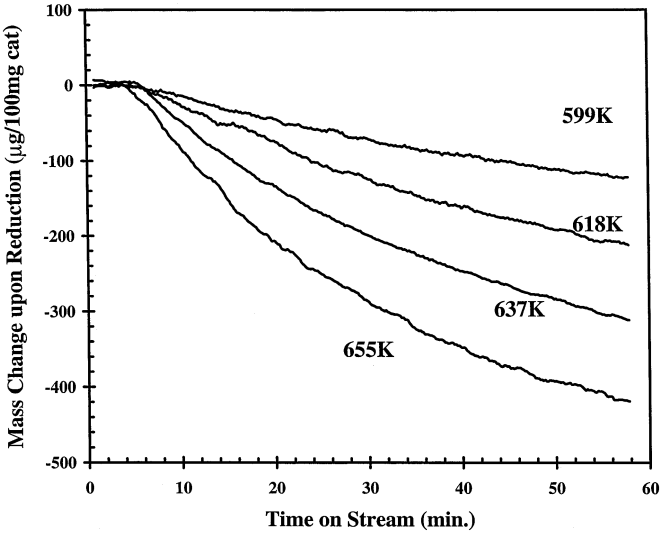

FIG. 6. Isothermal reduction of the reaction equilibrated VPO catalyst in 0.8 vol% butane (balanced in helium). Conditions: 100 mg VPO catalyst, SV = 30,000 ml h^{-1}(g cat)$^{-1}$, and temperature as indicated.

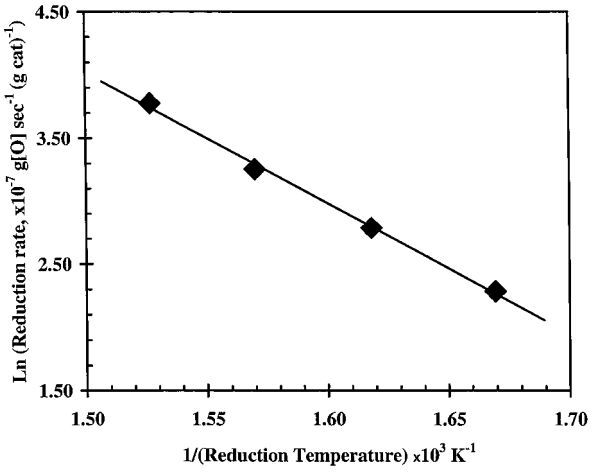

FIG. 7. Determination of the activation energy for the reduction of the equilibrated VPO catalyst.

butane concentration and remains constant under the experimental conditions for each curve in Fig. 4. Integration of Eq. [6] gives the following equations:

$$[O] = [O]_0 - \{f\ (T, [C_4H_{10}])/\psi\} \cdot t \quad \text{for } b = 0; \qquad [7]$$

$$[O] = [O]_0 \cdot \mathrm{Exp}(-\{f\ (T, [C_4H_{10}])/\psi\} \cdot t) \quad \text{for } b = 1; \qquad [8]$$

$$[O] = [O]_0 \cdot \left\{(b-1) \cdot \{f\ (T, [C_4H_{10}])/\psi\} \cdot t \cdot [O]_0^{(b-1)} + 1\right\}^{-1/(b-1)} \quad \text{for } b \neq 0, 1. \qquad [9]$$

$[O]_0$ is the initial lattice oxygen concentration in the equilibrated catalyst. Its meaning will be discussed latter.

According to the definition of mass change m, one can write

$$m = \psi \cdot \{[O] - [O]_0\}. \qquad [10]$$

Then, Eqs. [7]–[9] can be rewritten as relations of m versus time, t.

$$m = -\{f\ (T, [C_4H_{10}])\} \cdot t, \quad \text{for } b = 0; \qquad [11]$$

TABLE 4

Effect of Temperature on the Reduction Rate of the VPO Catalyst[a]

Reduction temperature (K)	Rate of reduction ($\times 10^{-7}$ g[O]s^{-1} (g cat)$^{-1}$)
599	9.8
618	16.2
637	25.9
655	43.6

[a] The reduction rate was measured from the slope of mass change at the beginning of the reduction. Reductant: 0.8 vol% butane in helium, 50 ml/min; Catalyst: 0.1 g $(VO)_2P_2O_7$.

$$m = \psi \cdot [O]_0(\exp(-\{f\ (T, [C_4H_{10}])/\psi\} \cdot t) - 1) \quad \text{for } b = 1; \qquad [12]$$

$$m = \psi \cdot [O]_0 \cdot \{\{[(b-1) \cdot \{f\ (T, [C_4H_{10}])/\psi\} \cdot t \cdot [O]_0^{(b-1)} + 1\}^{-1/(b-1)} - 1\} \quad \text{for } b \neq 0, 1. \qquad [13]$$

By combining the units used for mass change, m, and oxygen concentration [O] as well as the catalyst BET surface area of 16.9 $m^2 g^{-1}$, one can determine that the value of ψ is 270.

The experimental results in Fig. 4 showing the dependence of mass change, m, on time, t, are replotted in Fig. 8, using filled symbols for the data at the three butane concentrations used. A fit of m versus t with Eqs. [11] through [13] can determine b, $[O]_0$, and $f\ (T, [C_4H_{10}])$. The best fit was obtained with $b = 4$ and $[O]_0 = 3.67 \times 10^{-5}$ mol m^{-2}.

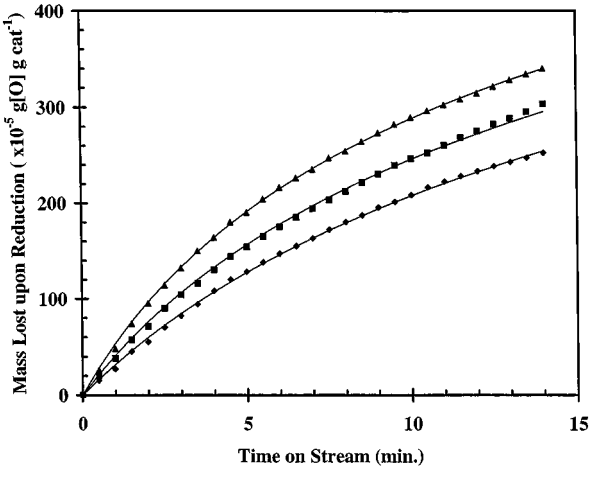

FIG. 8. Simulation of the reaction order on the lattice oxygen concentration. Conditions for the experimental data: 100 mg VPO catalyst, temperature = 400°C, SV = 30,000 ml h^{-1}(g cat)$^{-1}$; butane concentrations are as in Fig. 4.

TABLE 5

Values of $f\ (T, [C_4H_{10}])$ Determined by Curve Fitting from Fig. 8

Butane concentration (vol%)	$f\ (T, [C_4H_{10}])$
0.4	1.88×10^{14}
0.8	2.48×10^{14}
1.64	3.31×10^{14}

[a] Reaction temperature: 673 K; reactant is butane balanced with helium, 50 ml/min.

The solid curves in Fig. 8 are the results of such fitting. It can be seen that the fitting of the experimental data is extremely good.

The values of $f\ (T, [C_4H_{10}])$ obtained from each curve in Fig. 8 are listed in Table 5. According to Eq. [6], a good fit to the data should produce a dependence of $f\ (T, [C_4H_{10}])$ on $[C_4H_{10}]$ similar to the reaction order previously determined with respect to butane. Indeed, the plot of $\ln(f\ (T, [C_4H_{10}])$ versus $[C_4H_{10}]$ in Fig. 9 shows a reaction order of 0.4, exactly the same value as was obtained from Fig. 5. In other words, the reaction order in butane determined from the initial 100 s or less of the reduction transient appears to be valid for the entire duration of the transients shown in Fig. 8 (ca. 15 min).

In summary, the reduction of the equilibrated VPO catalyst in butane/He can be described with the rate equation

$$-dm/dt = 270(-d[O]/dt) = 4.9 \times 10^6 \exp(-85000/(RT))\,[C_4H_{10}]^{0.4}\,[O]^4, \quad [14]$$

where R is the gas constant 8.31 J mol^{-1} K^{-1} and the other terms have the following dimensions: $-dm/dt$: g(g cat)$^{-1}$ s^{-1}; $d[O]/dt$: mol m^{-2} s^{-1}; $[C_4H_{10}]$ = butane partial pressure, Torr; $[O]$ = lattice oxygen concentration, mol m^{-2} s^{-1}; T = temperature, K.

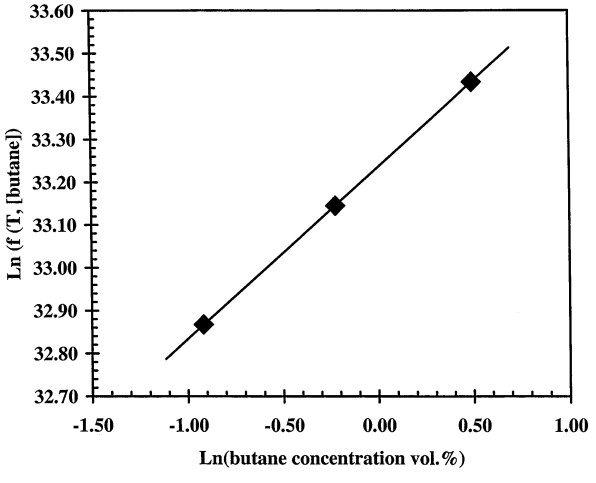

FIG. 9. Determination of reaction order on butane from the regressed data for f (for definition, see the text).

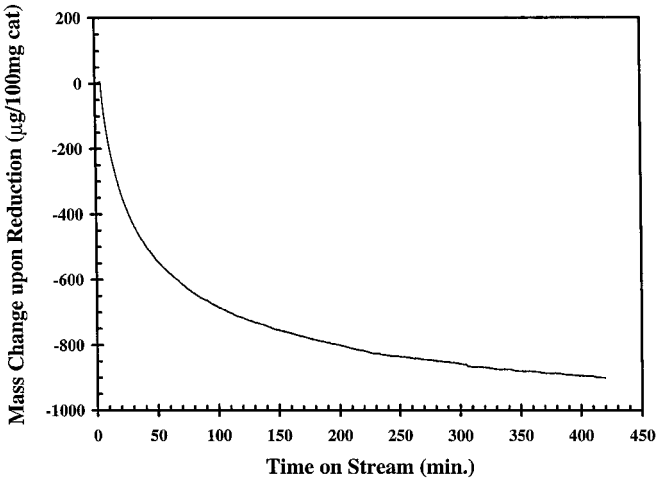

FIG. 10. Isothermal reduction of the reaction equilibrated VPO catalyst in 0.8 vol% butane (balance helium). Conditions: 100 mg VPO catalyst, SV = 30,000 ml h^{-1}(g cat)$^{-1}$, and temperature 400°C.

DISCUSSION

The Total Oxygen Capacity of the Equilibrated VPO Catalyst

Let us first look at the meaning of $[O]_0$. According to the definition, $[O]_0$ is the total reducible lattice oxygen concentration in the equilibrated VPO catalyst. Based on the regressed value for $[O]_0$, about 3.67×10^{-5} mol [O]m^{-2} can be removed from the equilibrated catalyst, corresponding to a total mass loss of 990 μg per 100 mg catalyst. To test this prediction, we conducted an extensive reduction of the equilibrated catalyst in 0.8 vol% butane at 400°C. The result is shown in Fig. 10. The total mass change for the 100-mg sample does indeed tend to level off between 900 and 1000 mg after reduction approaching 7 h.

Considering the surface area of the catalyst, 16.9 m^2/g, and assuming that the exposed catalyst surface is composed of mainly [100] crystal faces of vanadyl pyrophosphate with vanadium density of 8.4 μmol/m^2, one can compute that reduction of one monolayer of the catalyst from V^{5+} to V^{3+} should result in a total mass change of about 225 μg per 100 mg catalyst. That is to say the total oxygen capacity of 990 μg per 100 mg catalyst corresponds to the reduction of vanadium up to about five layers. The agreement of the predicted total oxygen capacity with the kinetic data obtained for removal of less than one-third of this amount indicates that the same kinetic model holds for the reduction by surface lattice oxygen and the subsurface oxygen. This result is in agreement with our previous finding that the reduction

of subsurface oxygen was not limited by lattice oxygen diffusion (9).

The unique redox properties of the VPO catalyst might be rationalized by an understanding of its nanostructure. Recently, Duvauchelle and Bordes studied the morphology of a vanadyl pyrophosphate crystal with TEM and XRD (37). They found that a typical vanadyl pyrophosphate prepared by calcination at 420°C is composed of a great number of small crystallites with average crystallite size of 437 Å (37). These crystallites are slightly misoriented with respect to each other. This mosaic of crystallites exposes one side to form the outer surface of the catalyst, the area of which is measured by the BET method. The other sides of the crystallites are obscured by adjacent crystallites and form the boundary surface between crystallite domains. Because of the misorientation between the domains, there may be a large number of defects at the boundary surface. These defect sites are very active and may serve as an oxygen reservoir during redox operation. Oxygen diffusion along these defective surfaces is sufficiently fast that, at any moment during a redox operation, the oxygen concentration at the boundary surface is in equilibrium with that on the outer surface of the catalyst and thus there is no lattice oxygen diffusion limitation to reduction. Because the crystallites expose one side (which is about 1/6 of their total surface) to the outer surface, the total area involved in the redox operation, including the boundary surface area, is about six times the BET surface area of the catalyst, which provides a total oxygen capacity of the VPO catalyst corresponding to several monolayers' reduction.

Implications for the Mechanism of Butane Oxidation on the VPO Catalyst

It has been proposed that the oxidation of butane to maleic anhydride under steady-state reaction conditions with co-fed butane and oxygen can be represented by the following redox scheme (10–13):

$$\text{Butane} + [\text{O}] \overset{K_\text{R}}{\rightarrow} [*] + \text{MA} + \text{CO} + \text{CO}_2 \qquad [15]$$

$$[*] + \text{O}_2 \overset{K_\text{O}}{\rightarrow} [\text{O}]. \qquad [16]$$

Under steady-state conditions according to Bej and Rao (10–13), the rate of butane consumption can be expressed as

$$-dP_\text{B}/dt = \left(K_\text{R} K_\text{O} P_\text{B}^s P_{\text{O}_2}^n\right) \big/ \left(K_\text{O} P_{\text{O}_2}^n + \alpha K_\text{B} P_\text{B}^s\right), \qquad [17]$$

where K_R and K_O are the rate constants for reactions [15] and [16], P_{O_2} and P_B are the partial pressures for oxygen and butane, respectively, s and n are the reaction orders for butane and oxygen, respectively. α is the number of moles of oxygen required to convert 1 mol of butane. The microbalance results showed that, under steady-state reaction conditions, the catalyst surface is in an oxidized state, i.e., the fractional surface coverage of oxygen is close to unity, thus $\alpha K_\text{R} P_\text{B}^s \ll K_\text{O} P_{\text{O}2}^n$. Accordingly, the above rate expression [17] can be written as

$$-dP_\text{B}/dt = K_\text{R} P_\text{B}^s. \qquad [18]$$

If one makes this simplification, the rate constant for the steady-state oxidation would be the same as the rate constant for the oxidation of butane with lattice oxygen. In fact, the experimental results show that the apparent activation for the steady-state reaction is 88 kJ/mol and the activation energy for the transient reaction of butane on the VPO catalyst is 85 kJ/mol. They are the same within experimental error. This suggests that under the conditions of our steady-state reaction experiments, the rate for the oxidation of butane on the VPO catalyst is determined by the activation of butane. Based on kinetic isotope effect measurements, Pepera *et al.* (38) concluded that the initial activation of butane by C–H cleavage is indeed the rate-determining step.

For the transient reaction of butane on the equilibrated VPO catalyst, the reaction rate is fourth order in lattice oxygen concentration. Such a high reaction order suggests that several lattice oxygen atoms are involved in the rate-determining step, activation of butane by the abstraction of hydrogen. Ziolkowski *et al.* studied the mechanism of butane oxidation on the VPO catalyst in terms of the crystallochemical model of active sites (39). They suggested that when butane is oxidized with the VPO catalyst, it is first adsorbed on the surface oxygen by two hydrogen bonds (C–H–O) involving the two terminal methyl groups; then, the two C–H bonds dissociate to form hydroxyl groups (–OH) and the two terminal carbons form C–O bonds to form a stable reaction intermediate. In this process, four lattice oxygen anions are involved, which may result in the fourth order dependence of the reaction rate on the lattice oxygen concentration.

Effective Oxygen Capacity

The total oxygen capacity of the VPO catalyst is as high as 990 μg per 100 mg catalyst, but it takes more than 7 h to make full use of it. In practice, the actual oxygen transfer capacity for cyclic redox operation is controlled by the kinetics and depends on the operating conditions. As an example, we can analyze the dependence of the effective oxygen capacity on the butane concentration in the reductant. Assume that the reduction time is 2 min and the operation temperature is 400°C, which are practical for the industrial application. From rate equation [14], we can obtain the following relation for the effective oxygen capacity M (μg/100 mg cat):

$$M = 990\left\{1 - (0.294[\text{C}_4\text{H}_{10}]^{0.4} + 1)^{-1/3}\right\}. \qquad [19]$$

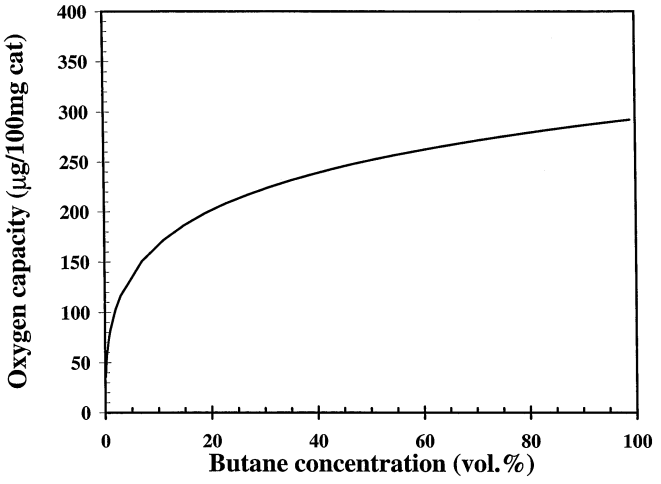

FIG. 11. Dependence of the effective oxygen capacity on butane concentration predicted with the kinetic model. Other conditions: temperature = 400°C, reduction time = 2 min.

The predicted values for the oxygen capacity are plotted in Fig. 11. These data show that if the circulating redox operation is not limited by the restoration of oxygen in the regenerator, the oxygen transfer rate can be increased by increasing the butane concentration in the reduction (riser) reactor. This dependence is strong for butane concentrations up to 10 vol%, but becomes less important above 20 vol%. Contractor reported a similar dependence for cyclic operation from pilot plant experiments (40).

CONCLUSIONS

The kinetics of the transient reaction of butane on the equilibrated VPO catalyst are well described by Eq. [14]. This rate expression can be used in the reactor design and the optimization of the operation conditions in a circulating fluidized reactor.

The similarity of the activation energy for the transient reduction reaction to that for steady-state butane oxidation on the same catalyst indicates that the rate of oxidation of butane under steady-state conditions with co-fed oxygen is determined by the activation of butane. The fourth-order dependence of the reduction rate on lattice oxygen concentration suggests that four lattice oxygen ions were involved in the activation of butane in the rate-determining step.

REFERENCES

1. *Chem. Eng. News*, **March 29**, 16 (1999).
2. Contractor, R. M., Bergna, H. E., Horowitz, H. S., Blackstone, C. M., Malone, B., Torardi, C. C., Griffiths, B., Chowdhry, U., and Sleight, A. W., *Catal. Today* **1**, 49 (1987).
3. Contractor, R. M., and Sleight, A. W., *Catal. Today* **1**, 175 (1988).
4. Contractor, R. M., and Sleight, A. W., *Catal. Today* **1**, 587 (1987).
5. Contractor, R. M., Garnett, D. I., Horowitz, H. S., Bergna, H. E., Patience, G. S., Schwartz, J. T., and Sisler, G. M., *in* "New Developments in Selective Oxidation II" (V. Cortes Corberan and S. Vic Bellon, Eds.), p. 233. Elsevier, Amsterdam, 1994.
6. Emig, G., Uihlein, K., and Hacker, C.-J., *in* "New Developments in Selective Oxidation II" (V. Cortes Corberan and S. Vic Bellon, Eds.), p. 243. Elsevier, Amsterdam, 1994.
7. Contractor, R. M., Horowitz, H. S., Sisler, G. M., and Bordes, E., *Catal. Today* **37**, 51 (1997).
8. Bordes, E., and Contractor, R. M., *Topics Catal.* **3**, 365 (1996).
9. Wang, D., Kung, H. H., and Barteau, M. A., *Appl. Catal. A* **201**, 203 (2000).
10. Bej, S. K., and Rao, M. S., *Ind. Eng. Chem. Res.* **30**, 1819 (1991).
11. Bej, S. K., and Rao, M. S., *Ind. Eng. Chem. Res.* **30**, 1824 (1991).
12. Bej, S. K., and Rao, M. S., *Ind. Eng. Chem. Res.* **30**, 1829 (1991).
13. Bej, S. K., and Rao, M. S., *Ind. Eng. Chem. Res.* **31**, 2075 (1992).
14. Suter, D., Bartroli, F., Schneider, F. D., Rippin, W. T., and Newson, E. J., *Chem. Eng. Sci.* **45**, 2169 (1990).
15. Schneider, P., Emig, G., and Hofmann, H., *Ind. Eng. Chem. Res.* **22**, 2236 (1987).
16. Wellauer, T. P., Cresswell, D. L., and Newson, E. J., *Chem. Eng. Sci.* **41**, 756 (1986).
17. Centi, G., Trifiro, F., Ebner, J. R., and Franchetti, V. M., *Chem. Rev.* **88**, 55 (1988).
18. Centi, G., Fornasari, G., and Trifiro, F., *Ind. Eng. Chem. Prod. Res. Dev.* **24**, 32 (1985).
19. Wahlfahrt, K., and Hofmann, H., *Chem. Ing. Tech.* **52**, 811 (1980).
20. Lerou, J. J., and Weiher, J. F., Paper presented at Pittsburgh/Cleveland Catalysis Society Meeting, May, 1986.
21. Buchanan, J. S., and Sundaresan, S., *Appl. Catal.* **26**, 211 (1986).
22. Johnson, J. W., Johnston, D. C., Jacobson, A. J., and Brody, J. F., *J. Am. Chem. Soc.* **106**, 8123 (1984).
23. Rekoske, J. E., and Barteau, M. A., *J. Phys. Chem. B* **101**, 1113 (1997).
24. Fung, S. C., Querini, C. A., Liu, K., Rumschitzki, D. C., and Ho, T. C., *in* "Catalyst Deactivation" (B. Delmon and G. F. Froment, Eds.), Vol. 88, pp. 305–312. Elsevier, Amsterdam, 1994.
25. Zhu, W., Van de Graaf, J. M., Van den Broeke, L. J. P., Kapteijn, F., and Moulijn, J. A., *Ind. Eng. Chem. Res.* **37**, 1934 (1998).
26. Bordes, E., *Catal. Today* **1**, 499 (1987).
27. Guliants, V. V., Benziger, J. B., Sundaresan, S., Wachs, I. E., Jehng, J.-M., and Roberts, J. E., *Catal. Today* **28**, 275 (1996).
28. Hodnett, B. K., Permane, Ph., and Delmon, B., *Appl. Catal.* **6**, 231 (1983).
29. Batiot, C., and Hodnett, B. K., *Appl. Catal.* **137**, 179 (1996).
30. Bordes, E., *Catal. Today* **16**, 127 (1993).
31. Okuhara, T., and Misono, M., *Catal. Today* **16**, 161 (1993).
32. Wang, D., Kung, M. C., and Kung, H. H., *Catal. Lett.* **65**, 9 (2000).
33. Ye, D., Satsuma, A., Hattori, A., Hattori, T., and Murakami, Y., *Catal. Today* **16**, 1,113 (1993).
34. Matsuura, I., *Catal. Today* **16**, 1,123 (1993).
35. Bej, S. K., and Rao, M. S., *Appl. Catal. A* **83**, 149 (1992).
36. Hutchings, G. J., *Appl. Catal.* **72**, 1 (1991).
37. Duvauchelle, N., and Bordes, E., *Catal. Lett.* **57**, 81 (1999).
38. Pepera, M., Callahan, J. L., Desmond, M. J., Milberger, E. C., Blum, P. R., and Bremer, N. J., *J. Am. Chem. Soc.* **107**, 4883 (1985).
39. Ziolkowski, J., Bordes, E., and Courtine, P., *J. Catal.* **122**, 126 (1990).
40. Contractor, R. M., *Catal. Today* **1**, 645 (1987).